REPORT DOCUMENTATION PAGE		Form Approved OMB No 0704-0188

1a REPORT SECURITY CLASSIFICATION UNCLASSIFIED	1b RESTRICTIVE MARKINGS
2a. SECURITY CLASSIFICATION AUTHORITY	3. DISTRIBUTION / AVAILABILITY OF REPORT
2b DECLASSIFICATION / DOWNGRADING SCHEDULE	Approved for public release; distribution unlimited.

4 PERFORMING ORGANIZATION REPORT NUMBER(S)	5 MONITORING ORGANIZATION REPORT NUMBER(S)
NRL Report 9228	

6a NAME OF PERFORMING ORGANIZATION Naval Research Laboratory	6b OFFICE SYMBOL (If applicable) 8310	7a. NAME OF MONITORING ORGANIZATION
6c. ADDRESS (City, State, and ZIP Code) Washington, DC 20375-5000		7b ADDRESS (City, State, and ZIP Code)

8a. NAME OF FUNDING / SPONSORING ORGANIZATION Office of Naval Research	8b OFFICE SYMBOL (If applicable)	9 PROCUREMENT INSTRUMENT IDENTIFICATION NUMBER

8c. ADDRESS (City, State, and ZIP Code) Arlington, VA 22217	10 SOURCE OF FUNDING NUMBERS			
	PROGRAM ELEMENT NO 61153N	PROJECT NO	TASK NO	WORK UNIT ACCESSION NO DN180-016

11 TITLE (Include Security Classification)

Remote Sensing of Evaporation Ducts for Naval Warfare

12 PERSONAL AUTHOR(S)
Geernaert, G. L.

13a TYPE OF REPORT Final	13b TIME COVERED FROM 1/88 TO 1/89	14. DATE OF REPORT (Year, Month, Day) 1989 November 14	15 PAGE COUNT 30

16 SUPPLEMENTARY NOTATION

17 COSATI CODES			18 SUBJECT TERMS (Continue on reverse if necessary and identify by block number)
FIELD	GROUP	SUB-GROUP	Sea surface temperature fronts; Atmospheric refractivity; Evaporation ducting; Radar holes; Radar propagation.

19 ABSTRACT (Continue on reverse if necessary and identify by block number)

For the Navy warfare posture, the sensing of both strategic and tactical environmental data support is required to adequately map the ocean and atmosphere for maximum advantage in operational planning and management. To achieve these ends, concentrated R&D in key areas must be accomplished, especially the appropriate mix of sensors, their data fusion, and innovative applications on warfare systems and/or for their use as tactical decision aids. Areas critical to military operations are the prediction and application of atmospheric refractivity gradients. There are two classes of refractivity we must understand: ionospheric plasma processes and lower atmospheric thermal/humidity effects. We describe the use of the evaporation duct over the ocean and a plan for obtaining information about the evaporation duct by space-borne sensors.

Since pre-World War II days, there has been keen interest in understanding and predicting the nature of long range electromagnetic wave propagation in the lower and upper atmospheres. This interest rapidly evolved toward examining

(Continues)

20 DISTRIBUTION / AVAILABILITY OF ABSTRACT ☒ UNCLASSIFIED/UNLIMITED ☐ SAME AS RPT ☐ DTIC USERS	21 ABSTRACT SECURITY CLASSIFICATION UNCLASSIFIED	
22a NAME OF RESPONSIBLE INDIVIDUAL G. L. Geernaert	22b TELEPHONE (Include Area Code) (202) 404-7230	22c OFFICE SYMBOL Code 8310

DD Form 1473, JUN 86   Previous editions are obsolete.   SECURITY CLASSIFICATION OF THIS PAGE

19. ABSTRACT (Continued)

propagation models, atmospheric structures, and natural ambient conditions associated with refractivity. While many efforts that focussed on upper atmospheric refraction examined both homogeneous and nonhomogeneous conditions, research on the theory and modeling of lower atmospheric refractivity, particularly evaporation ducts over a nonhomogeneous ocean, has staggered over the past five decades.

Much is known about surface layer similarity theory and propagation model techniques, but little attention has been placed on the spatial variabilities in the turbulent propagation medium (such as the atmospheric surface layer) in regions of strategic Navy interest. Specifically, these regions include the coastal shelf, Gulf Stream, marginal ice zone, and those places where sharp sea surface temperature fronts exist. For tomorrow's Navy, using remote sensing techniques to infer evaporative and tropospheric ducts are a requirement, to provide an edge in antisubmarine warfare, antisurface warfare, antiair warfare, and strike warfare—particularly in support of battle-group management and long-range [cruise] missile deployments. Although research efforts on ducts must couple the tropospheric and surface layer components, this report summarizes the state of the art for the evaporative duct and assesses the potential of new and future results on improving next generation naval warfare capabilities.

An analysis of tropospheric ducts will not be addressed in this report and will therefore need to be addressed under a separate cover; this report evaluates only surface-based evaporation ducts.

DD Form 1473, JUN 86 (Reverse)

CONTENTS

iii

REMOTE SENSING OF EVAPORATION DUCTS FOR
NAVAL WARFARE

1. INTRODUCTION

Early in this century, when ham radio enthusiasts discovered skip zones and found that anomalous atmospheric conditions produced unusual reception, little was known about the ionosphere, propagation characteristics, or irregularities in atmospheric density. The quality of shortwave reception (up to about 50 MHz) exhibited diurnal regularity, which we now attribute to the solar influence on ionospheric structure. Radio waves in the range of 100 to 10,000 MHz were sometimes found to be received at unusually long distances and these over-the-horizon propagation characteristics were attributed to tropospheric stable layers and, therefore, downward curvature of radio waves. Unexplained long range propagation generated scientific curiosity to investigate reasons and applications for waveguides and ducts. For communications, establishing the most appropriate set (distribution and spacing) of relay links needed to be known; for the military, atmospheric conditions that produced radar holes needed to be evaluated. Most of the early work on ionospheric and tropospheric ducting (and the associated climatology) was conducted during the World War II years, 1938 to 1948. The reports published by Bell Laboratory, RCA Laboratory, and Radiation Laboratories (Rad Lab) describe our understanding of ducts during these years (Kerr 1951).

The results from the 1940s produced considerable uncertainty in predicting signal strength with distance whether one was propagating over land or ocean. Since little was known of atmospheric turbulence, the efforts during the 1950s were focussed on turbulence generation and decay and described the mean atmospheric profiles that influence radio propagation, in particular, explaining the troposcatter that was blamed for signal degradation. These atmospheric theorists and experimentalists developed programs that were coupled to other scientific problems, such as diffusion, wind-wave generation, and air-sea interaction. Major groups were spawned at the Air Force Geophysics Laboratory, the University of Hamburg, the University of Dresden, the Pennsylvania State University, the Commonwealth Scientific and Industrial Research Organization (CSIRO), Australia, and the University of Washington, among others. Little work was done on ducting during the 1950s; instead, the focus was placed on methods, techniques, and instrument development to understand the nature of the propagation medium (primarily, micrometeorology research). This research was devoted to understanding such phenomena as elevated and surface layer windspeeds, temperatures, humidity gradients, Kelvin-Helmholtz instabilities, inversion characteristics, and modeling.

During the 1960s, with new advances in turbulence research, reemphasis was placed on ducting characteristics, especially the evaporative duct, particularly at Naval Electronics Laboratory Center (NELC) in San Diego, Rad Lab, Nippon Telephone/Telegraph Corporation, and the University of Hamburg. Although many data sets were collected worldwide (the Irish Sea, Tokyo Bay, southern California coast, Cape Cod, and others), the Hamburg group developed the most comprehensive program. This program monitored propagation in the evaporative duct over a more open ocean environment at a 77-km distance across the North Sea and at four frequencies (6.8 GHz, 2.3 GHz, 566

MHz, and 160 MHz) (Brocks 1965). NELC conducted many one-to-two-week experiments over coastal water bodies, however their advances were overshadowed by those made in the Hamburg group. The Naval Research Laboratory (NRL) and Johns Hopkins University/Applied Physics Laboratory (JHU/APL) conducted sporadic research on ducts during this time.

In the 1970s, NELC and Naval Environmental Prediction and Research Facility (NEPRF) compiled and transitioned the two decades of results into 6.2 and 6.3 programs. Naval Ocean Systems Center (NOSC) and NEPRF jointly devised the Refractive Effects Guidebook (REG), in which synoptic typing was used to associate certain refractivity profiles with climatological patterns; the REG, however, cannot readily predict realistic evaporative ducts. Richter (1979), on the other hand, produced a set of codes to support the Integrated Refractive Effects Prediction System (IREPS) Program. This code predicts the most likely propagation characteristics on both a climatological and regional basis given a radiosonde profile. In collaboration with NEPRF, the Fleet Numerical Oceanography Center (FNOC) subsequently developed a coupled atmospheric and ocean prediction system in which surface evaporative duct heights were calculated from coarse input and forecast data. Output predictions by the FNOC models are generally based on large scale horizontal homogeneity using their current code. The use of their current code has produced uncertain results in many sharp baroclinic regions, such as the Gulf Stream, sea surface temperature frontal regions, and/or the marginal ice zone.

Basic research programs designed to couple ducting with new micrometeorological results were established in the 1970s at the U.S. Naval Postgraduate School (NPGS) and NEPRF, both in Monterey, CA, and in the 1980s at JHU/APL, as well as defense labs in the Netherlands and West Germany, among others. As in the research conducted during the 1960s by the Hamburg group, the European efforts used offshore towers as experimental sites. The NPGS efforts in the 1970s were unique because they coupled air-sea interaction with traditional micrometeorology theory. It then became more widely accepted that varying degrees of surface wave energetics severely impact the description of surface layer refractivity profiles. In the Soviet Union, atmospheric refractivity investigations on electromagnetic (e.m.) propagation were reported in the open literature by researchers at the Institute of Atmospheric Optics (Omsk, USSR) and the Radiophysical Institute (Sevastopol, Ukraine). Soviet efforts were more theoretical in nature.

Currently, United States research on propagation models through refractive gradients are conducted at NRL, NOSC, and JHU/APL. The JHU/APL focusses its program on lower atmospheric propagation modeling techniques (Dockery and Konstanzer 1987). Both NPGS and NEPRF concentrate their research efforts on planetary boundary layer turbulence measurements and m deling, while NOSC maintains its niche as propagation experimentalists and develops models for use Navy fleet operations.

2. THE NAVY NEED

The military advantage of understanding the nature of ducts became immediately apparent after the development of radar. Like over-the-horizon and anomalous ducting of radio waves observed by ham operators, Navy operators at sea must know the extent to which a radar can detect incoming aircraft, vehicles, or missiles on or near the surface. In the presence of an evaporation duct, transmissions can be used to both detect and be detected. With the current capabilities in remote sensing, it may be the Navy operator's choice to avoid transmitting in the evaporation duct, particularly if remotely sensed information is readily available.

2

Of particular importance in battle group management is the development of radar holes. These holes can occur when the ship-based radar transmitter is near or below the evaporative duct height and a wide-beam transmission is used. Figure 1 shows that a gap will appear in radar coverage in which hostile missiles or aircraft can enter undetected. The danger is that smart systems built into aircraft or missiles can be coded into battle group operations plans, where the height of the calculated evaporation duct using remotely sensed information can provide a tactical advantage. Defensive action therefore dictates that the Navy operator must be aware of this possibility, and targeting must be prioritized for those elevation angles most susceptible to undetected intrusion.
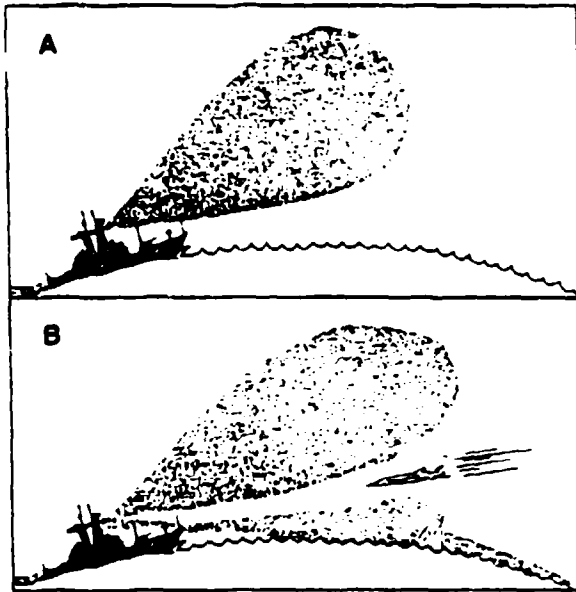

Fig. 1 — Shipboard radar coverage under normal atmospheric conditions: (a) no ducting; and (b) changes in the presence of an evaporation duct. Under ducting conditions, an aircraft in the radar hole cannot be seen by the ship's radar (Thompson 1987).

Offensive aircraft and/or long-range missiles have two choices of defensive actions to minimize detection. If an evaporation duct exists near the surface (and most likely also a radar hole), the smart system must evaluate the degree of sea clutter and the presence of inversion-based stratus (to prevent detection by optical and infrared spaceborne sensors) and must determine the most appropriate height to reach in order to be within the radar hole. In the event of no evaporation duct (a condition that can be inferred by using remotely sensed information), the aircraft may be required to ascend above the planetary boundary layer (PBL) inversion. For cruise missiles, optimal heights can be determined by knowing the sea clutter characteristics and the nature of local sea surface temperature fronts that produce natural false echoes at ship-based microwave frequencies.

The existence of an evaporation duct may permit the detection of surface ships at extreme range when the range limitation is due to atmospheric stability and wind stress (similar to windspeed) variability along the propagation path. Sea surface temperature variability induces stratification variation and, therefore, variability in the refractive profile, while wind stress acts as a generator of background clutter. Little is known about natural variability or spatial scales associated with these two geophysical parameters, but intuitively one would expect a strong relationship of variations on such easily measured quantities as the prevailing wind direction (because of its relation to storm sector), air pressure tendency, and nearness to a major surface feature (coastline, Gulf Stream, etc.).

3

G. L. GEERNAERT

Evaporation duct intensity is additionally important to conduct over-the-horizon (OTH) radar operations and communications; particularly important is the prediction of appropriate radar frequencies and the optimum transmission height to maximize the interpretation of radar backscatter and range limitations. In support of signal and electronic intelligence operations, identifying anomalous signals in the presence of sea clutter is especially important for both low and zero (horizontal) angle antenna pointing within a highly refractive medium. Spatial variability of evaporative and tropospheric ducts as a function of stability class, mesoscale turbulence, and the variability in surface waves and temperatures have an impact on describing the statistical reliability of signal propagation. This reliability can be evaluated with a multidiscriplinary research approach that couples atmospheric, ocean surface, and mixed layer processes predicting statistical constraints on the reliability of weapons systems under adverse meteorological and/or oceanographic conditions.

As a next effort to develop a better understanding of surface based ducts, the Navy may proceed on several courses: (1) develop a theoretical basis that can be coupled to new and/or existing ocean surface remote-sensing programs that use air-sea interaction theory, oceanography, meteorology, and a suite of radar sensors; (2) establish an ongoing database using results from basic and applied investigations; (3) develop algorithms applicable to space-based, surface-based, and aircraft sensors, which infer the appropriate environmental information needed to predict duct heights, particularly in regions where Navy ships or submarines engage in battle (sea surface frontal regions, marginal ice zone, lee of atmospheric storms), and (4) develop an imbedded smart system for aircraft and/or missiles whereby the code can be developed to predict elevation and width of a radar hole for tactical advantage in offensive or defensive operations.

The following sections summarize the state of the art in surface layer refraction and turbulence theory and describe the development of the above four steps. However, refinement of the steps requires study of satellite remote sensing of ocean surface features. A discussion follows on the expected behavior of surface-based ducts over sea-surface temperature fronts; finally, we discuss a first order approach for using remote-sensing active and passive sensors and techniques to infer surface duct information.

3. SURFACE LAYER REFRACTION

We approach the evaporation ducting problem by concentrating on turbulence in the lowest 50 to 100 m of the planetary boundary layer, that is, immediately above the sea surface. The surface layer is characterized by a common set of turbulence scaling laws that simplify the transition of theory into practical modeling of refractive features. Refraction in the surface layer, unfortunately, requires detailed information on the temperature and humidity gradients along the path of a propagating e.m. wave. Although horizontal homogeneity is implicit to the scaling laws, realistic ducting of e.m. waves must evaluate spatial perturbations to the equations of motion caused by sea surface temperature variability.

To treat refraction from a practical viewpoint, we briefly review the physics of e.m. propagation and then consider the nature of the propagating medium, that is, turbulent features within the surface layer. In the latter, we emphasize the study of homogeneity in the propagating medium and then evaluate the extent to which surface layer inhomogeneity criteria must be built into ducting research.

4

3.1 Refraction Theory

When an electric field impinges on a gaseous medium composed of polar and nonpolar molecules, the polarizability $\tilde{P}$ of a gaseous medium under the influence of a fluctuating electric field of frequency ω is

$$\tilde{P} = \{(\epsilon - 1)/(\epsilon + 2)\} M/\rho, \tag{1}$$

where ϵ is the dielectric constant, M the molecular weight, and and ρ the air density. Defining α_0 as the average polarizability of the gas molecules, N as Avogadro's number, k as the Boltzmann constant, and T as air temperature, Eq. (1) may be rewritten as

$$\tilde{P}(\omega) = 4 \pi N/3 \{\alpha_0 + \mu^2/3kT (1 + 1/i\omega\tau)\} \tag{2}$$

where μ is the permanent dipole moment and τ is the relaxation time required for the external field-induced orientations of the molecules to return to a random distribution after the field is removed. See Debye (1957) for a complete derivation and treatment of Eq. (2).

If the external field has an imposed frequency < 100 GHz and noting that ϵ is of order 1, Eq. (2) becomes

$$\epsilon - 1 = 4\pi N M^{-1} \rho (\alpha_0 + \mu^2/3kT). \tag{3}$$

For nonpolar gases, the second term on the right-hand side (rhs) of Eq. (3) disappears and by using the perfect gas law, Eq. (3) can be approximated as

$$\epsilon - 1 = K_1' (P/T), \tag{4}$$

where K_1' is a constant. For polar gases, Eq. (3) may be written

$$\epsilon - 1 = K_2' (P/T)(A + B/T), \tag{5}$$

where K_2', A, and B are constants.

Since the refractive index n is defined as $(\mu/\epsilon)^{1/2}$, the refractivity N for the atmosphere becomes

$$N = (n - 1) \times 10^6 = K_1 (P/T) + K_2 (e/T) + K_3 (e/T^2) + K_4 P_c/T), \tag{6}$$

where the first term on the rhs is due to the dry nonpolar partial pressure, the fourth term is due to carbon dioxide, and the middle two terms are due to water vapor. See Bean and Dutton (1966) for a more detailed review of the derivations. Based on experimental evidence, Eq. (6) is reduced to a more practical form by

$$N = 77.6/T (P + 4810 e/T), \tag{7}$$

5

where the air pressure P and specific humidity e are expressed respectively in millibars and degrees Kelvin.

Following Snell's law, the differential bending of an e.m. wave $d\hat{\tau}$ along the ray path is

$$d\hat{\tau} = -(dn/n)\cot \theta, \tag{8}$$

where θ is the ray elevation angle with respect to the horizontal plane. Kerr (1951) extended this result for the case where the gradient of n lies in the vertical plane

$$d\gamma/ds = |\nabla n| \sin \gamma/n, \tag{9}$$

where γ is the angle between the ray and $-\nabla n$. Martin and Wright (1963) generalized the ray refraction problem for horizontal variations in n where

$$d\hat{\tau}/ds = 10^{-6} n^{-1} (-\partial N/\partial z \cos \gamma + \partial N/\partial x \sin \gamma), \tag{10}$$

where n and N are related by Eq. (6)

In the case of a sloping inversion base (or any N surface), Eq. (10) implies that

$$|\nabla n| \cos \psi = \partial n/\partial z, \tag{11}$$

$$|\nabla n| \sin \psi = \partial n/\partial x, \tag{12}$$

where ψ is the angle of the N surface with respect to the Earth's surface. Clearly, from Eqs. (9 through 12), the ray trace is subject to the slope of the N surface, both at the inversion base and in the evaporation region near the surface.

Differentiating N and retaining important terms, one easily obtains

$$\partial N/\partial x = -A(P/T^2)\partial T/\partial x + (B/T^2)\partial e/\partial x, \tag{13}$$

$$\partial N/\partial z = -A(P/T^2)\partial T/\partial z + (B/T^2)\partial e/\partial z - APg/RT^2, \tag{14}$$

where $A = 77.6$ C/mb and $B = 3.73 \times 10^5$ C/mb. In Eq. (14), the third term on the rhs was evaluated by assuming the surface layer to be in hydrostatic balance and using the ideal gas law; R is the gas constant. The impact of a sea-surface temperature (SST) front on $|\nabla T|$ and $|\nabla e|$ will be simulated by considering the turbulence modification as air is advected across an SST front; we address this special case in a later section.

From Eqs. (11 through 14), temperature and humidity profiles within the surface layer are seen to strongly influence the e.m. wave refraction. Since refraction is a local phenomenon, we must examine the mean state for simplicity, for example, temperature and humidity mean profiles, and follow

with an indication of the variability of profiles over the open ocean. In general, research on ducts assumes homogeneity; the horizontal gradients (in Eq. (14)) are therefore assumed in spatially homogeneous regions to be unimportant. This horizontal homogeneity criterion breaks down in the surface layer over sea-surface temperature fronts where internal boundary layers can form and often exhibit slopes that can exceed 10% (the horizontal gradient of refractivity can exceed 10% of the vertical gradient of refractivity). In this context, we focus our attention (in Section 4) on regions where variability overlaps regions that are strategically important to the Navy.

3.2 Surface Layer Theory

The windspeed, temperature, and humidity gradients in the surface layer over a marine surface may be represented (after Panofsky and Dutton 1984) as

$$dU/dz = u^*/kz \; \phi_M(z/L), \tag{15}$$

$$dT/dz = T^*/kz \; \phi_T(z/L), \tag{16}$$

$$dq/dz = q^*/kz \; \phi_q(z/L), \tag{17}$$

where U is the mean windspeed, and the specific humidity q is related to the partial pressure of water vapor by

$$q = 0.622 \; e/P. \tag{18}$$

The quantities (u^*, T^*, and q^*) represent scaling quantities and act as indicators for the wind stress, heat flux, and humidity flux. We represent these later in the report by using easily measured quantities (such as windspeed, temperature difference, and humidity difference.) The stratification functions ϕ identically equal unity for neutral stability; for unstable stratifications, they are less than unity and are greater than unity for stratified flow. These functions have been parameterized as

$$\phi_M = \begin{cases} (1 - 16 \, z/L)^{-1/4} & ; \text{unstable} \\ \\ 1 + 5 \, z/L & ; \text{stable} \end{cases}, \tag{19}$$

$$\phi_T = \begin{cases} \phi_M^2 & ; \text{unstable} \\ \\ \phi_M & ; \text{stable} \end{cases}, \tag{20}$$

and

$$\phi_q = \phi_T \tag{21}$$

7

where in Eqs. (19 and 20) the stability parameter L (the Monin-Obukhov length) is defined according to the sensible and latent heat fluxes (scaled respectively with T^* and q^*) by

$$L = T u^{*2}/(gk\{T^* + .61Tq^*\}).$$

(22)

It must be pointed out that the numerical constants "5" and "16" found in Eq. (19) were both determined from measurements collected over land (Panofsky and Dutton 1984); Geernaert (1989) has argued that over water these constants can be significantly larger.

The friction velocity u^* and the temperature and humidity scales T^* and q^* are generally approximated by bulk formulations as

$$u^{*2} = C_D U^2,$$

(23)

$$u^*T^* = -C_T U (T_0 - T),$$

(24)

$$u^*q^* = -C_E U (q_0 - q),$$

(25)

and C_D, C_H, and C_E are, respectively, the coefficients for drag (or wind stress), sensible heat, and moisture transfer. These coefficients have values on the order of 10^{-3} and depend on stratification and sea state. Quantities with "0" subscripts indicate surface values, while others conventionally represent the 10-m elevation above the surface. (T_0 is referred to in this report as the SST).

It is useful at this point to mention that u^*, T^*, and q^*, in their true forms, are turbulent covariances, and the use of Eqs. (23 through 25) introduces an error because of approximations that use easily measured quantities. A primary reason for such inherent errors is that mean values are assumed to be related to turbulent fluctuation intensities—a relation that alone generates some degree of uncertainty. This uncertainty is generally incorporated in the coefficients $C_{D,H,E}$ in Eqs. (23 through 25); in Section 3.5 we see that these uncertainties are on the order of 30%.

Since the stratification functions depend critically on the specified values for u^*, T^*, and to a much smaller degree q^*, we must specify the dependence of the three bulk coefficients on the environmental quantities. Because of difficulties in experimentally measuring the sensible and latent at fluxes, constant values for C_H are usually reported as a function of either positive or negative stratification; based on Smith (1980), we use values of 1.08×10^{-3} for unstable flow and 0.86×10^{-3} for stable stratifications. Because experimentally determined values of C_E exhibit large scattering, a constant value of 1.30×10^{-3}, with no statistical dependence on stratifications, has been suggested by Anderson and Smith (1981).

The drag coefficient is well known to adjust for stratification according to

$$C_D = [k^{-1} (\ln\{z/z_0\} - \psi_M)]^{-2},$$

(26)

where k is the von Karman constant ($= .4$) and z is the sampling height. The roughness length z_0 has been empirically related to wave state (after Geernaert et al. 1987) in the form

$$z_0 = z \exp(-3.65 [c_0/u^*]^{2/3}), \qquad (27)$$

where c_0 is the phase speed of the dominant locally generated gravity wave. (A subtle distinction in drag coefficient formulations is emphasized in Section 3.5.) The ratio c_0/u^* has typical values for steady conditions of ~25 to 30. In the region upwind of an SST front, the wind stress and surface wave spectrum are generally in an equilibrium state, but on the downwind side, the wave field is either under- or overdeveloped because of the wind stress adjustment as the air column undergoes a step change in thermal stability. The adjustment of air flowing over a colder surface is always much more severe than flow in the opposite direction.

The profile stratification function ψ_M found in Eq. (26) is parameterized in terms of ϕ_M and is generally written as

$$\psi_M = \begin{cases} 2 \ln([1 + \phi_M^{-1}]/2) + \ln([1 + \phi_M^{-2}]/2) - 2 \tan^{-1}\phi_M^{-1} + \pi/2; & \text{unstable} \\ -5 \, z/L & ; \text{stable} \end{cases} \qquad (28)$$

The accurate prediction of u^* is critical in defining the Monin-Obukhov length L, which in turn, is required to calculate the stratification functions. Stratification functions are not so important unless one is near either SST fronts or a coastal shelf, where surface temperature changes induce functional jumps in thermal stability. Otherwise, in the open ocean, the key ingredients to surface layer ducting lie in specifying realistic humidity and windspeed profiles, while air-sea temperature differences generally lie close to zero.

The elaborate development of the surface layer equations shown above (the scaling laws) is critical to defining the surface-based evaporation duct height (Section 3.3). Using these equations becomes important when examining regions where step changes in sea surface temperature fronts occur, for instance, near the Gulf Stream. The equations developed here allow us to illustrate duct height calculations over homogeneous and/or nonhomogeneous stratifications.

3.3 Evaporation Duct Height

Combining Eqs. (14 through 25) provides a form for the vertical gradient of the index of refraction, as

$$dN/dz = -(AP/T^2)(T^*/kz)\phi_T + (B/T^2)(q^*/kz)\phi_q - .0321 \, m^{-1}. \qquad (29)$$

Given that the Earth's curvature implies a gradient of N with the local normal to the flat Earth's surface to be $-.157 \, m^{-1}$, the duct height is estimated by defining $dN/dz = 0$ and rearranging Eq. (29) into a more operational form by showing

$$Z = 17.9 \, T^*\phi_T - 85.8 \, q^*\phi_q, \qquad (30)$$

where the numerical coefficients in Eq. (30) carry units for pressure in mb, temperature in the vicinity of 290 K, and $Z = z$.

Referring to Eq. (30), we can use bulk relations to easily predict the duct height by using measured windspeeds, temperatures, and humidity. Therefore, in Eqs. (20 through 22), T^* and q^* may be rewritten as

$$T^* = -C_T C_D^{-1/2}(T_0 - T),$$ (31)

$$q^* = -C_E C_D^{-1/2} (q_0 - q).$$ (32)

Given the experimentally determined values for the exchange coefficients in Eqs. (23 through 25), we write

$$T^* = .029 \, \Delta T$$ (33)

$$q^* = .043 \, \Delta q,$$ (34)

where ΔT and Δq are respectively the air-sea temperature and air-sea humidity differences. We note here that the numerical coefficients in Eqs. (33) and (34) rely on an appropriate choice of drag coefficient. Since this quantity depends on stability, wave state, and windspeed, some specification of this quantity is in order to refine the prediction of Z; uncertainty and errors are addressed in Section 3.5.

The humidity at the surface is always assumed to be 100% (the surface humidity is considered to be identically related to the saturation water vapor pressure associated with the SST). Equation (18) relates the specific humidity q to the vapor pressure e. The air humidity is similarly related to the saturation vapor pressure with respect to the air temperature (or with Eq. (18), also the saturation specific humidity) according to

$$q = r \, q_s$$

where r is the measured relative humidity.

For a horizontally homogeneous surface layer with a zero air-sea temperature difference, (neutral stratifications—assuming humidity is far less important in stability than for refraction), the problem is greatly simplified, and Eq. (30) reduces to

$$Z = -85.8 \, (.043) \, (q_s - rq_s).$$ (35)

Since q^* is proportional to $(q - q_0)$, the neutral evaporative duct height depends on r; we now have

$$Z = 3.7 \, q_s \, (1 - r),$$ (36)

where q_s is the saturation specific humidity in units of (gm/kg) for the given SST and Z is in meters. Typical values of r are 60% to 80%.

The variability of Z because of SST for neutral stabilities is now described by using the Clausius-Clapeyron equation for the specific humidity, and we obtain

$$q_s = .00764 \exp(18.905 - 5350/T), \tag{37}$$

where temperature is in degrees K.

Coupling Eq. (37) with Eq. (36) and noting that q in Eq. (36) is in (g/kg), we easily arrive at a key equation to illustrate the dependence of surface duct height on r and SST by

$$Z = 27.9 \, (1 - r) \exp(18.905 - 5350/T). \tag{38}$$

For Navy applications, the primary interest now is how we can use Eq. (38) to roughly estimate the importance of these ducts in a tactical environment. Note that Eq. (38) is developed to illustrate this point; it is by no means a perfect solution to our problem. Note also that even though a 30% uncertainty is built into Eq. (38) the trends and variabilities shown in Table 1 are very real. In the author's opinion, the uncertainty will be systematically reduced when air-sea interaction investigators understand the dependence of the drag, heat, and moisture exchange coefficients on wave state. The wave-state dependence is not included in Eq. (38); the importance of waves is raised in a later section.

With Eq. (38), we can get an idea of how large the duct heights are by examining the range of sea surface temperatures naturally observed. Considering this, we devised Table 1, which shows that the evaporation duct height in meters depends on SST and r, where the SST's used are selected according to regions that are tactically important to Navy operations.

Table 1 — Duct Height (in m) Depending on SST and r

		Relative Humidity			
	SST (°C)	$r = 20\%$	$r = 40\%$	$r = 60\%$	$r = 80\%$
Subarctic	5	15.9	11.9	7.9	4.0
Coastal	10	22.3	16.7	11.2	5.6
Sargasso Sea	20	42.6	31.9	21.3	10.6
Gulf Stream	25	57.8	43.4	28.9	14.5
Persian Gulf	30	77.8	58.3	38.9	19.4

For lower windspeeds, the values for Z will likely be slightly larger because the drag coefficient exhibits an increasing dependence on windspeed (Eq. (41)); also we used a constant drag coefficient to provide the illustration in Table 1 (see Section 3.4 for more details).

Table 1 shows that warm sea surface temperatures, particularly in regions such as the Persian Gulf, the Gulf Stream, and Kuroshio, exhibit deep surface evaporation ducts because of their high surface water temperatures. For low flying aircraft and/or missiles, considering the duct height (particularly over warm surfaces) has obvious strategic and surveillance consequences.

3.4 Trapped Radar Frequencies

Based on Bean and Dutton (1965), the minimum e.m. frequency that can be trapped within an evaporation (or any surface-based duct) depends on the duct height according to

$$f(\text{min}) = 360.33 \, Z^{-3/2}, \tag{39}$$

where $f(\text{min})$ and Z are respectively in GHz and m. Since the radar frequency used by ships (for antiair warfare (AAW) and surveillance) is X band, we can, for the sake of analysis, select 10 GHz as a test frequency to evaluate the usefulness of ship radars in using the evaporation duct. Inverting Eq. (39), and substituting $f = 10$ GHz, we obtain

$$Z > 1.95 \, \text{m}, \tag{40}$$

as the condition of X-band trapping. For practical purposes, all evaporation ducts are > 1.95 m unless one is in a sea fog where RH = 100%. In this environment, a special case arises.

This exercise shows that in the presence of sea fog, a layer will exist above the foggy layer where an evaporative layer exists. Further, sea fogs generally occur where surface-based temperature inversions exist under stable and light wind conditions; in this case, the evaporation duct will be augmented by a strong, positive temperature gradient, thereby producing an even deeper surface-based duct.

So far, we have concentrated mainly on the evaporation contribution to the surface-based duct, that is, the evaporation duct. The temperature contribution will prevail during nonneutral conditions or mainly during low windspeed conditions and/or large-scale thermal advection, which usually occur away from a coastline. In the case of nonneutral stratifications, thermally unstable conditions produce upward refraction and therefore subtract from any contribution based on humidity. Thermally stable conditions, on the other hand, add to the intensity of a surface-based duct.

The state of the art for the temperature contribution to Z is that slightly unstable conditions are fairly well understood based on experimental measurements over land; few measurements have been collected over the ocean. Stable stratifications are poorly understood, particularly over the ocean, in terms of ducting characteristics. Recent measurements collected during Frontal Air-Sea Interaction Experiment (FASINEX) and under analysis at Scripps Institute of Oceanography will likely provide more insight on stable stratification and boundary layer adjustment. More study is required to evaluate this problem.

3.5 Error Analysis

Given the assumptions and the experimental data that determined the set of coefficients for Table 1, we now evaluate the uncertainty in the calculations. At this point, we step back to Eq. (30) which defines the surface duct height. Two numerical coefficients in Eq. (30) are based on an assumed mean temperature on the order of 290 K, a von Karman constant of 0.4, and otherwise near-universal constants. For the sake of error analysis, the SST varies by no more than perhaps 5% about a mean of 290; and the von Karman constant has an uncertainty of perhaps 5%. Together these coefficients exhibit, at most, 15% variability, which is well within any criteria we may use for ducting applications.

The difficulty in using Eq. (30) for operational purposes, unfortunately, lies in the evaluation of the quantities T^* and q^*. Recalling Eqs. (31 and 32), the combination of the drag coefficient with the heat and moisture exchange coefficients needs particular attention in the context of their respective statistical uncertainties. The drag coefficient C_D has been evaluated by Geernaert et al. (1987) both in its dependence on windspeed and wave state, with an additional review of its dependence on stability. The neutral dependence on windspeed is shown by

$$10^3 \, C_{DN} = .0847 \, U_{10} + 0.577, \tag{41}$$

where Eq. (41) applies to a horizontally homogeneous surface, windspeed measurement at 10 m above the surface, and neutral stratifications (with the subscript DN indicating neutral drag).

The same data that described Eq. (41) were analyzed in terms of wave age, and a parallel relation was proposed by

$$C_{DN} = .0123 \, (C_0/u^*)^{-2/3}, \tag{42}$$

where C_0 represents the phase speed of the dominant locally generated ocean-surface gravity wave. Use of Eq. (42) in lieu of Eq. (41) must be applied in regions where wind stress and wave state adjustment occur on the lee side of a significant SST front and/or after a sudden change in windspeed or fetch. In Section 4, we use Eq. (42) for the special case of flow over a sea surface temperature front—the regions that do not meet the horizontal homogeneous criterion.

The relationship between the drag coefficient C_D found in Eq. (26) and its neutral counterpart found in Eqs. (41) and (42) is

$$C_{DN} = (C_D^{-1/2} + \psi_M/k)^{-2}, \tag{43}$$

where ψ_M is the profile stratification function in Eq. (28). The important distinction between Eqs. (42) and (43) rather than using Eq. (41) with Eq. (43) is that the neutral drag coefficient on the cold side will always be lower than its counterpart on the warm side of an SST front. This new result is based on theoretical arguments (Geernaert et al., 1987) and has been experimentally verified during FASINEX by Li et al. (1988). Different C_{DN}'s on adjacent sides of SST fronts imply that the differences in duct heights on the two sides of the front will be even greater than previously expected. Figure 2 is a graphic display of Eq. (43).

Although we have briefly described how the drag coefficient depends on wave state, little has been mentioned in the open literature about how the heat and humidity coefficients depend on wave state. Clearly, both the heat and humidity exchanges depend on the surface spray and foam, but no statistical study has yet been conducted that provides insight on how to reduce the uncertainty in the predicted duct heights. Improvements in duct height predictions will depend (in part) on results from the Humidity Exchange Over the Sea (HEXOS) Experiment (Katsaros et al. 1987); see Geernaert (1989) for a review of recent work.

To find the most exact estimate of the evaporation duct height (for spatially homogeneous conditions), one must couple Eq. (30) and Eqs. (20 through 22), (41), (43), and (44), and specify the
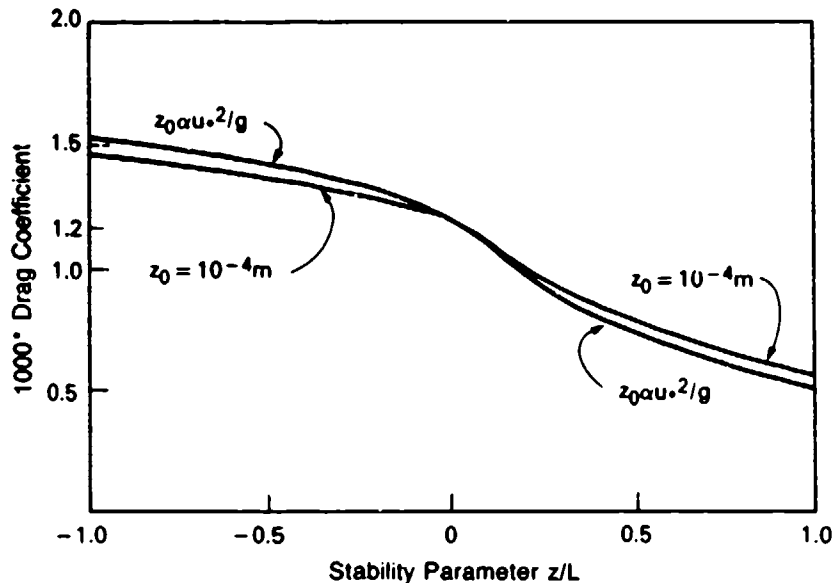
Fig. 2 — Dependence of the drag coefficient on the stability parameter, z/L (where z = height and L = Monin-Obukhov length; $L < 0$ is unstable, $L > 0$ is stable). The difference between the two lines is statistically insignificant and represents two methods of specifying the roughness length.

values of C_H for unstable and stable stratifications and C_E. By taking this more exact approach, we can estimate the errors within T^* and q^* based solely on uncertainties in the stability corrections and reported values of the drag coefficient, heat exchange coefficient, and moisture exchange coefficient.

Typical uncertainties in the drag coefficient are 20%, while for the temperature and moisture coefficients, uncertainties are typically reported to be closer to 30%. For the evaporation duct, this translates into an uncertainty in both T^* and q^* on the order of 40%. (In the opinion of the author, deviations in all three coefficients are linked to some degree, therefore making the uncertainty of 40% an upper limit; it is most likely closer to 30%.) By using the most recent air-sea interaction experimental results, this uncertainty directly translates into the same uncertainty in the calculated duct height Z. Since relative uncertainties in the coefficients are smaller than their absolute uncertainties, accuracy in the predicted duct height differences over SST fronts may be more useful than evaluating their absolute heights. (Of course, one ideally would like to know both.)

4. SPECIAL CASE: FLOW OVER SST FRONTS

Focusing one's attention on regions such as SST fronts presents a challenge to evaluating e.m. wave propagation. On the front's upwind side, fetches are often long enough that the surface layer above the air-sea interface is in near-equilibrium with the surface-wave field and SST. While this equilibrium is generally associated with near-neutral stratifications, the change in SST across such a surface front immediately changes the air-sea temperature difference thereby inducing a change in the thermal stability of the lower air column. This change in thermal stability reduces the wind stress (and lowers the wave state) if the downstream SST is colder. Conversely, if the downstream SST is warmer, the air becomes less stable and more turbulent thereby increasing the stress and wave height. The change in stress across the front is a consequence of the strong dependence of the drag coefficient

14

on thermal stratification. As indicated in Table 1, the predictions assume a fixed value for the drag coefficient and even further assume that the stratifications are neutral (no air-sea temperature difference and making $T^* = 0$).

For flow from neutral to stable (towards colder water), the downwind surface-based duct will be driven by both the positive temperature profile and the lower surface humidity associated with the colder surface temperature; the complication here requires the equations relating the profiles to be coupled with their stratification functions. Unfortunately the parameters become intertwined, and the set of equations iterate to a final solution. This iteration becomes similarly dependent on sea state since the phase speed of the dominant wave remains semiconserved for a large distance across the front (even though its wave height reduces because of the drop in stress, that is, C_o/u^* increases as u^* decreases, and C_o remains constant, Eq. (42).

For flow in the opposite direction (towards a warmer SST), the humidity gradient will increase since the SST is higher and consequently so also is the surface saturated vapor pressure; recall that the relative humidity at the surface is 100%. The advected air above the warmer water will retain the same moisture content. This results in a greater difference in humidity between the surface and air and an increase in q^*. The corresponding air-sea temperature difference will act to destabilize the air column and subtract from the refractivity produced by the humidity profile (the evaporative duct). Very little change in duct height is obtained by combining the set of equations and considering changes in both T^* and q^*. Figure 3 illustrates these conditions.
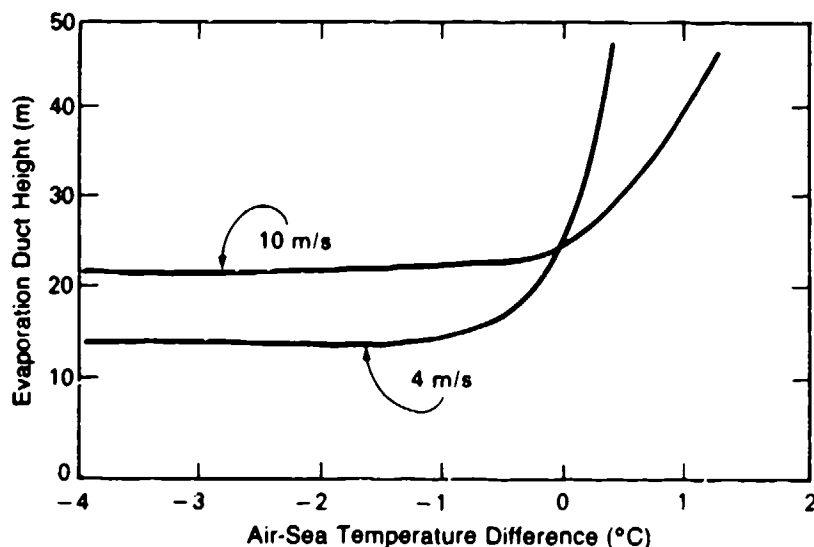

Fig. 3 — Calculation of the evaporation duct height for given windspeeds of 4 and 10 m/s and air-sea temperature difference as a variable. The calculations simulate a constant air temperature and wave phase speed, relative humidity of 75%, and median SST of 25°C. All upwind conditions are neutral and steady state.

Similarly, the minimum trapped radar frequency will have a response to the flow. This is particularly important if future radar systems used on ships are able to step the frequency down through L band. Figure 4 shows that an L-band e.m. wave propagating over an SST front will not be ducted in the surface layer on the downstream side if the windspeed is low and/or the relative humidity is high and given that the downstream side has a warmer sea surface temperature.
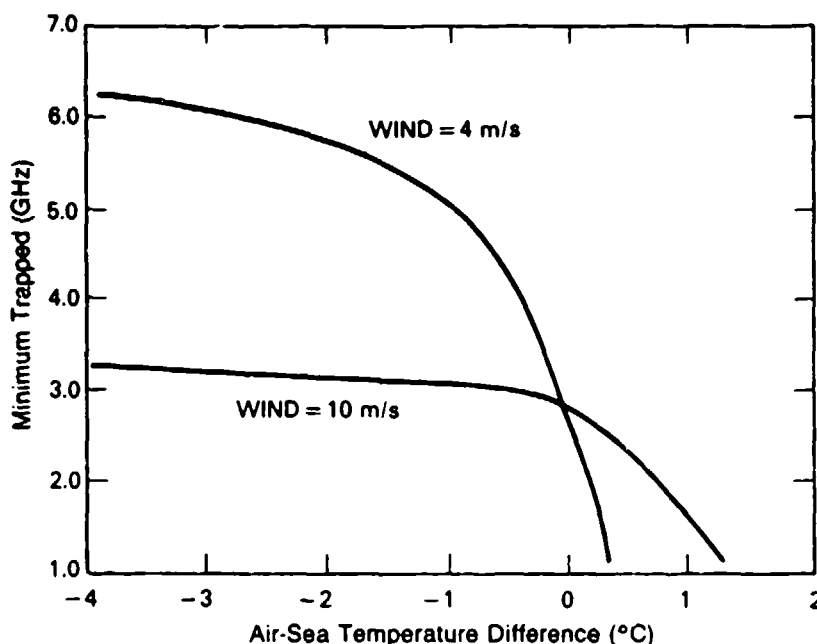

Fig. 4 — Predicted minimum trapped radar frequency (GHz) downwind of the SST front (for a Δ SST of 4°C) as a function of windspeed and sign of the SST change (wind direction). Air temperature is 25°C; humidity is 75%.

The process of total lower atmospheric adjustment across an SST front is of particular concern. This process is not well understood, and few data sets from over the ocean exist to support modeling efforts. Since the dynamics of surface layer coupling with the boundary layer are complex even in steady-state and horizontally homogeneous regions, research conducted over SST fronts is open for investigation. Most investigations conducted during the recent years have used stack patterns in which aircraft do profiling by flying 10-km (or more) segment lengths at many altitudes within the lower atmosphere (as was conducted during FASINEX). The PBL has a depth on the order of 1 km, roughly 10 times deeper than the surface layer. The information gained from the studies has been mostly qualitative, but the most important conclusion drawn is that the full boundary layer rapidly adjusts to changes in sea surface temperature. It must be pointed out that data from Norwegian Coastal Sea Experiment (NORCSEX-88) by Johannessen et al. (1989) are yielding similar changes in SST as well as large changes in both current shear and windspeed; the NORCSEX-88 measurements indicate that both windspeed and current exhibit dramatic changes over short distances (on the order of 1 km) across the coastal shelf west of Norway.

The physical response of the boundary layer over SST fronts is driven by a modified surface layer turbulence structure within the surface layer that manifests itself in modifying the energetics of the full boundary layer immediately downwind of the SST front. Depending on the wind direction

with respect to the front, the boundary layer will grow or decay, resulting in a sloping inversion base in the transition PBL immediately above the front. The greatest slope will most likely exist when the wind is nearly parallel to the front, thereby producing two boundary layers that are closely spaced above the SST front, each with different energetics and inversion heights. Since this transition PBL above the front can exhibit large slopes, the impact of inversion slope was examined with respect to radar range and em propagation; see Schleher (1982) and Barton (1973). In both these studies, inversion slopes on the order of 2 to 5 m/km were enough to cause serious range degradation due to upward refraction out of the waveguide and/or false echoes.

Figure 5 illustrates boundary layer adjustments over SST fronts. Using airborne lidar observations of the aerosol backscatter coefficient over the Gulf Stream wall (reported by Goroch et al. 1983), the inversion-level slope was demonstrated to increase on the warm side of the Gulf Stream at a rate of 5 m/km. Figure 5 points out the consequences of the adjustment process, particularly in cases where winds are light and dramatic changes in stability can develop. In this case of light winds, a small increase in SST of perhaps 2°C can cause a neutrally stratified flow to transform into near convective instability, particularly if the SST front is sharp (as does occur at the wall of the Gulf Stream, over the coastal shelf west of Norway, and in the marginal ice zone).
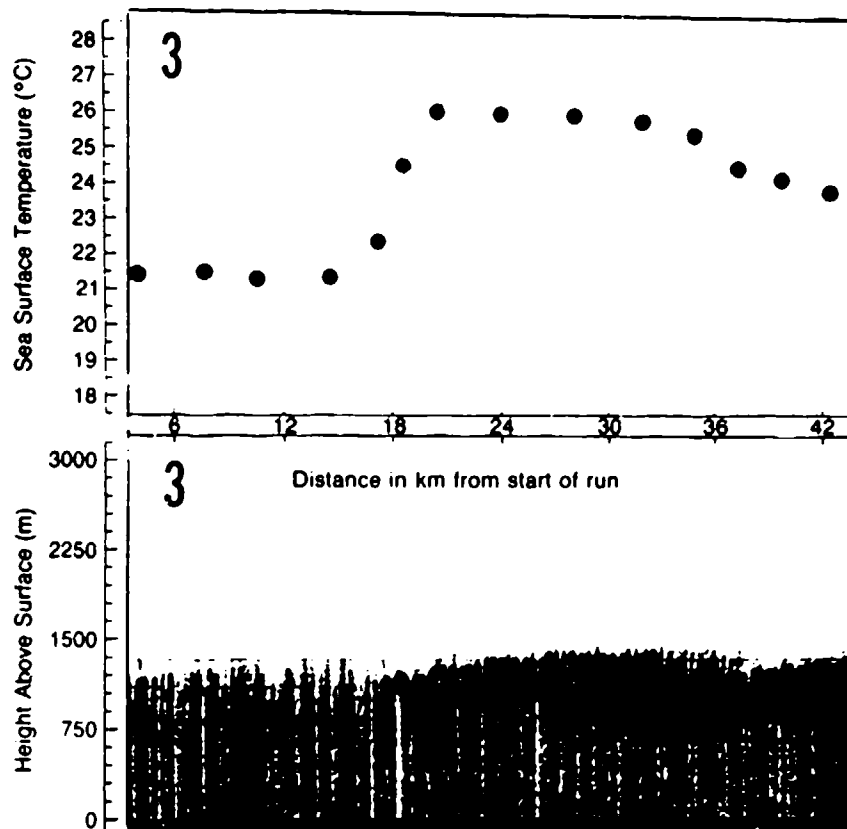

Fig. 5 — In the upper panel, the time series of the sea surface temperature (°C) using a downward-looking radiometer (Δ SST = 5°C); in the lower panel, downward-looking lidar scattering within the boundary layer. Vertical scale is in m in the lower panel while the horizontal intervals correspond to 10 km each. Data were collected by Goroch et al. (1982) by using the NOAA P-3 aircraft.

17

Our emphasis in this section has been on illustrating problems concerning tropospheric ducts rather than surface-based adjustment. There is simply no adequate spatial coverage of surface-layer turbulence that has been experimentally measured and reported, in part because of the difficulty in collecting such measurements over SST fronts. We can, for now, make theoretical predictions (Figs. 3 and 4) based on the body of experimental data available for different stratification classes and simply apply these results to the two adjacent boundary layers, each with different stratifications above the sea surface frontal zone. Coupling the equations again, we obtain a set of predictions for the changes in duct height and minimum trapped radar frequency. Clearly, the larger the SST jump across the front, the larger the change; the greatest differences will always occur when the wind flows towards colder water. Flow towards colder water stabilizes the air column and reduces the natural turbulence levels that provide kinetic energy to both the surface layer and the full PBL.

Since inversion level adjustment and inversion slopes can be blamed on signal degradation, the same observations can be extrapolated to the surface layer adjustment immediately above the air-sea interface. Based on experimental work conducted near airports, the adjustment of the surface layer to step-changes in roughness (experiments mostly conducted by the FAA near airports) yielded internal boundary layers with slopes of 10%. Slopes such as these are significantly larger than those observed by either Schleher or Barton. Even more severe problems in transmission refraction/losses and/or false echoes in the surface layer could be expected when compared to the same at the inversion atop the PBL. Again, these surface-based slopes will manifest themselves in describing the evaporative duct, especially over such regions as the Gulf Stream.

5. REMOTE SENSING TECHNIQUES FOR INFERRING EVAPORATION DUCTS

An evaluation of theory and measurements of surface layer response, ducting characteristics, and boundary layer response is a useful exercise for understanding the physics over nonhomogeneous surfaces, but the operational navy needs remotely sensed background environmental information as input data to gain accurate predictions. An R&D atmospheric and propagation effort must therefore be coupled with methods to use available and proposed passive and active microwave sensors (space-borne or flown on aircraft or missiles) to get a first crack at prediction. Now we will focus on (1) space-based remote sensing opportunities, and (2) sensing by instruments placed on missiles or aircraft flying within the boundary or surface layer.

5.1 Space-based Environmental Sensing

The current sensors defined for operational use with space platforms include:

- a low-frequency microwave radiomenter (LFMR);
- a special sensor microwave imager (SSM/I);
- an altimeter, ALT;
- a six-antenna scatterometer, NSCAT;
- an oceanographic synethetic aperture radar (SAR); and
- an advanced very high resolution radiometer (AVHRR).

18

Note that the LFMR has not been deployed. While both NSCAT and oceanographic SAR are not currently operational, predecessors of each were deployed on SEASAT. Both the AVHRR and SSM/I are currently operational sensors on the Defense Meteorology Satellite Program (DMSP) satellites, and the ALT is the primary sensor aboard GEOSAT.

For the study described here, the LFMR, NSCAT, and SSM/I are the important sensors. The LFMR was designed to infer sea surface temperature on roughly 6-km spatial scales with nearly all-weather capability. The SSM/I has the capability to infer total water vapor content as well as estimate the wind speed (not direction); the SSM/I additionally is designed to provide rainfall rate. The NSCAT provides not only wind speed but also direction. Except for the SAR, all the sensors have a surface footprint size on the order of 10 km; the oceanographic SAR is capable of fine-scale interpretation on the order of 100 m.

Clearly, for applications near sea surface fronts (such as coastal shelves and the Gulf Stream), the LFMR is a primary sensor required for evaluating evaporation ducts, radar holes, and inversion-based ducts. The LFMR provides information on both the absolute magnitude and variability of SST. The degree of SST change has both strategic and tactical operational value, particularly in connection with the ability to communicate acoustically across the front and/or in operational ASW surveillance. The SST additionally influences the degree of stratification change induced on the downstream boundary layer, thereby affecting the PBL inversion slopes and internal boundary layer slopes within the surface layer. These in turn can be used to determine the statistical chance of observing a false echo by using a ship-based OTH radar directed across the SST front. The character of the SST front (with its respective currents and shears) can be used also to describe the stability of the adjacent water mass and horizontal heat transport.

To evaluate the ducting problem, the LFMR however cannot act alone; the SST patterns must be coupled with the wind speed in the region and even more importantly it must be determined whether the wind is flowing towards warmer waters or towards colder waters. This distinction is reiterated, since flow towards warmer water has minimal impact when compared to the more severe effects when the wind blows in the opposite direction. With today's DMSP satellites, wind vectors can be estimated by using SSM/I fields overlayed with surface pressure analyses predicted at FNOC.

For on-line duct information processing, a scatterometer must be used and, if available, a SAR to provide fine-scale variability. The scatterometer system can provide this information on a coarse scale, but a SAR can isolate variabilities of backscatter intensity (such as wind speed) within the scatterometer footprint. Radar experiments have been conducted over SST fronts during FASINEX and NORCSEX; Fig. 6 illustrates a 4 dB drop in backscattered power during steady winds blowing from warm to cold water.

One can relate scatterometer cross-section measurements to the air-sea environment by noting that they are related to the wind stress according to

$$\sigma_0 = G(\alpha, \beta) + H(\alpha, \beta) \ln u^*, \qquad (45)$$

where the G and H functions are empirically derived to depend on the azimuth and incidence angles α and β, respectively; σ_0 is the normalized radar cross-section. Data such as those presented in Fig. 6 have been analyzed in terms of u^* by Li et al. (1988), and there is strong support now for applying NSCAT measurements in SST regions for directly predicting the wind stress with high confidence
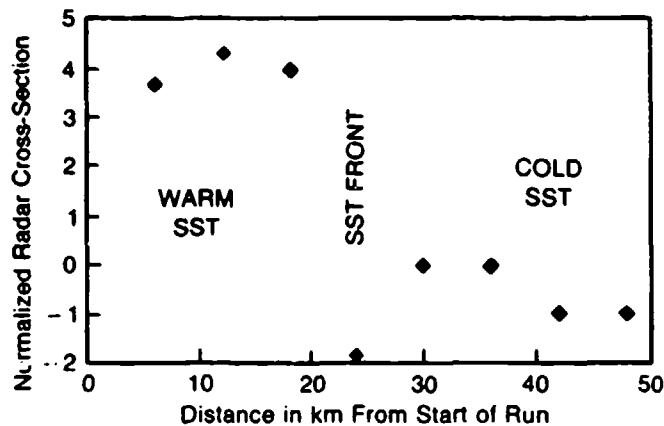
Fig. 6 — Time series of normalized radar cross section (in dB) across a sea surface temperature front (order of 3°C) on 16 February 1985 during FASINEX. Winds are 6 m/s and blowing towards colder water (Geernaert et al. 1988).

with instrumented aircraft. A problem still remains however if one wants to use SEASAT-type algorithms for inferring wind vectors from space; this problem does not rest so much in the model function interpretation as with model function inversion, spatial smoothing, and ambiguity removal over sets of 25-km (or greater) scatterometer footprints. The basis for this criticism is that even if the windspeed remains steady within a given footprint, the change in u^* on the two sides of the front will induce inhomogeneity in radar backscattered power where the footprint contains an SST front, thereby creating difficulty in evaluating the proper wind direction. For problems concerned with improving technology and environmental predictability in support of Navy operations, the R&D community must consider this caveat.

In Eq. (36), a first cut at predicting the evaporative duct height on the upwind side can be made by incorporating the NSCAT (so the upwind direction is known) and the LFMR, which provides the SST and therefore the saturation humidity by means of the Clausius-Clapeyron equation, Eq. (37). But what about the relative humidity r found in Eq. (36)? The relative humidity is typically on the order of 60% to 80%; but any uncertainty in this value, particularly near a desert region where small values of r can exist (such as the Persian Gulf) can produce a wide margin of error; see Table 1.

Smolinsky (1988) recently presented results that use passive radiometers, such as the SSM/I, to predict both the total water vapor and relative humidity within the PBL. This analysis assumes that nearly all of the water vapor is confined below the PBL inversion, and one must therefore estimate the depth of the boundary layer and the total columnar water vapor that is assumed to be within it. The SSM/I currently is capable of providing estimates of all these required quantities as long as surface conditions are horizontally homogeneous, both within and beyond the 12-km spatial footprint of the SSM/I. For regions where surface discontinuities exist (for instance, in the presence of SST fronts), the SSM/I cannot act alone as the sole sensor, but finer scale information is needed (by using an oceanographic SAR) as is the direction of the wind (by using a scatterometer). For the horizontally inhomogeneous surface, calculating the PBL depth Z_{PBL} is an important parameter to estimate locally, particularly for estimating the spatial variability of relative humidity. To first order, the PBL height is estimated by

$$Z_{PBL} = c \, u^* / f, \tag{46}$$

20

where c is an experimentally determined constant on the order of 0.3, and f is the Coriolis parameter (on the order of 10^{-4} s^{-1} in midlatitudes). Radar backscatter, obtained with an oceanographic SAR, can provide the fine-scale variability in $u*$ required in inhomogeneous regions (in the vicinity of SST fronts).

For operational algorithms, Eq. (46) can easily be coupled with Eq. (45); we now obtain a dependence of PBL height on the NSCAT or SAR cross sections (while noting that the NSCAT will provide more exact estimates of the area-averaged wind stress vector while the SAR provides an estimate of the finer scale magnitude variability) by

$$Z_{PBL} = c(c_3 - G)/Hf. \tag{47}$$

An alternate to Eqs. (46) and (47) would be to use the $u*$ estimates from brightness temperatures evaluated from the SSM/I system aboard the DMSP satellite (Smolinsky 1988), while noting the limitation imposed by the horizontal homogeneity requirement.

Since the surface layer energetics on the upwind side of an SST front are generally long fetch and horizontally homogeneous, data fusion by oceanographic SAR and either SSM/I or NSCAT information will provide a first-order calculation of the relative humidity estimates that are needed to calculate the most probable duct heights (on the upwind side), Eq. (37). On the downwind side of the SST front, a nonlinear adjustment of surface fluxes and surface layer profiles as well as wave state will occur. This downwind adjustment can be modeled in a first-order fashion by treating the downstream air mass with a new stability yet retaining the overlying wind vector as a constant. A more exact treatment of the adjustment process on the downwind side of the SST front, however, must consider the coupling between the decaying (or growing) wave state and the decrease (or increase) in heat flux, whereby the internal boundary layer associated with the step change in SST is considered.

By treating the upwind side as uniformly homogeneous and neutrally stratified, we can estimate the evaporative duct height information with Eq. (36). If a radar hole exists on the upward side, it will be immediately above the height Z. Some distance beyond the downwind side of the sea surface temperature front, assuming the wind vector remains steady, Eq. (30) must be used to estimate the new height Z given the new air-sea fluxes of humidity and temperature. For those occasions and/or places where the stratifications are not neutral on either the upwind or downwind side (for instance, when $T*$ is nonzero) coupling satellite remote sensing data with an atmospheric forecast database (by FNOC or the National Meteorology Center (NMC/NOAA)) should provide a dramatic improvement to evaporative duct height estimates. It is important to point out that sensors are being developed to measure temperature profiles from space (the SSMT and its next generations), but these temperature-measuring systems are designed to provide greater accuracy in the middle troposphere and higher. Temperatures near the surface are well within the PBL, and the PBL contains water vapor and often clouds that reduce the reliability of spaceborne high-resolution microwave sensors in providing near-surface information.

For remote sensing of evaporative duct heights from space or aircraft, we have been concentrating on either the open homogeneous ocean or over SST fronts. A key region worth mentioning is the marginal ice zone (MIZ), particularly since this region has inherent strategic and tactical interest. Degradation of electro-optical systems in the subarctic can easily be attributed to the same processes one observes over SST fronts, particularly the change in stratification and, therefore, resulting sloping

inversion, internal boundary layer, and turbulence structure as one transects the MIZ. Geernaert et al. (1989) reported that during particular wind conditions (especially on ice flow), very steep boundary layer slopes can develop, and systematic false echoes should be expected during these conditions. There has been scanty experimental work and even less theoretical work in either basic and applied research in understanding or predicting propagation across the MIZ. To make progress in R&D specifically for the MIZ, the data base requirement for such studies would involve both ground truth and the fusion of SAR, scatterometer, SSM/I, and LFMR data by aircraft and/or blimps and final coupling with sensors on space-based satellites.

5.2 Remote Sensing from Low Flying Projectiles or Aircraft

For stratetic and tactical operations, assuring that one wants a long-range projectile or low flying aircraft to remain within a radar hole (above the surface-based evaporative duct), inference of the local duct height would provide useful information especially to evaluate the probability that the low flying vehicle will be undetected by land or ship-based radar surveillance. To make real-time estimates of duct height onboard the vehicle with in situ sensors and/or links to a database satellite telemetry, the smart system onboard the low flying vehicle would require real-time measurements of air and water temperature, relative humidity, and flight altitude. Having air and water temperature and humidity provides an estimate of Z by coupling Eqs. (30) (33), and (34). Note that, unlike estimates of evaporative ducts from space-borne systems, inferring the duct height by using on-line in situ sensors from within the boundary layer will not require information on the wind vector that was required to model the surface layer adjustment across the sea surface temperature front. (Recall that the use of windspeed was critical for space-based sensing since the footprint size was so large that one needed to know the change of stability across an SST front, which can be modeled by assuming a wind vector to estimate the change in stability. The advantage of in situ low level sensors is that the stability does not need to be modeled but instead is measured in real-time.)

What sensors are required for the smart system flying within the boundary layer? Since it is low in the atmosphere, clouds are nearly always above the vehicle, so a simple downward-looking microwave radiometer can provide an estimate of the SST. Air temperature can be inferred by using a thermistor, while the relative humidity would need to be measured by trapping air samples and by using traditional techniques and/or a Lyman-alpha system.

6. SUMMARY

The application of remotely sensed information that yields estimates of radar holes can provide a tactical advantage in the survivability of cruise missiles, aircraft detection, and general surveillance. Also, space-based environmental information can provide estimates of ducting variability, and eventually, upon transitioning the R&D to higher categories, developmental codes can be produced that can assess the reliability of signal vs false echo. Existing technology, coupled with technology generated within the past half decade, is capable of providing the Navy an R&D program to improve our knowledge of radar holes and how they can be used by Navy weapons programs and systems. Clearly, this R&D will have tactical use if the research provides a survivability advantage for long-range weapons and low flying aircraft, that is, in support of surveillance and communications over SST fronts and/or in the subarctic far from strategic/tactical military support. The scientific and engineering concepts require the use of not just one sensor but the use of data fusion techniques from a suite of sensors to achieve this end.

The prospects lie in improved antiair warfare (AAW), antisurface warfare (ASUW), and antisubmarine warfare (ASW) operations. The problem of sea clutter was not discussed but clearly it plays an important part, since it is a function of u^* and therefore also a function of the scatterometer cross section. At this point, remote sensing of evaporation ducts requires:

- a research effort to establish both the turbulence modification across step changes in stratification for SST fronts and the subarctic, where additional information on changes in roughness and the statistical turbulence field on all spatial scales is required;

- the simultaneous propagation modeling over variable turbulence conditions and, in particular, sloping refractive zones;

- the applied use of space sensors to yield accurate information on atmospheric humidity, and for large footprints, the statistical variability of clouds within footprints; this variability impacts the interpretation of both active and passive microwave data collected from space, and

- a feasibility study to incorporate the technique described here for implementation on the Cruise Missile (and future long-range missile) Program; such a study provides the cruise missile with a smart system that allows it to fly in a region by minimizing its detectability; this smart system should also be evaluated by down-linking space-based estimates of tactical environmental information.

Developing operational codes by using sensors on the DMSP (especially the SSM/I) can provide an initial database simulation and sensitivity studies. The expertise in Navy laboratories currently includes meso- and macro-scale ocean and atmospheric modeling (including eddies), coupled air-ocean modeling, hydrodynamics, boundary layer meteorology, and the use of space systems designed to evaluate environmental variability for use in ASW, AAW, and C^3I. The transitional opportunities of such R&D would be directly linked to future IREPS codes and next-generation Tactical Environmental Support System (TESS).

7. ACKNOWLEDGMENTS

The author acknowledges both Andy Goroch (NEPRF) and Lew Wetzel (NRL) for providing memorandums discussing, respectively, the R&D on on tropospheric ducting at NEPRF and FNOC, and references on the development of the field, starting five decades ago.

8. REFERENCES

Anderson, G., and S.D. Smith (1981), "Evaporation Coefficient for the Sea Surface from Eddy Flux Measurements," *J. Geoph. Res.* **85**, 443-452.

Barton, I.A. (1973), "The Importance of Tilted Layers in the Tropospheric Ducting of Radio Waves Over the Timor Sea," *Radio Sci.* **8**, 727-732.

Bean, B.R., and E.J. Dutton (1966), *Radio Meteorology*, NBS Monograph 92, U.S. Government Printing Office.

Brocks, K. (1965), "Models of the Troposphere Derived from Direct Measurements of the Atmospheric Refractive Index," *Progress in Radio Science 1960-1963*, Vol. 2 (Elsevier Scientific Publishing Company, Inc., New York).

Dockery, G.D., and G.C. Konstanzer (1987), "Recent Advances in the Prediction of Tropospheric Propagation Using the Parabolic Equation," *JH/APL Tech Digest* 8(4), 404-412.

Debye, P. (1957), *Polar Modecules* (Dover Press, New York).

Geernaert, G.L., S.E. Larsen, and F. Hansen (1987), "Measurements of the Wind Stress, Heat Flux, and Turbulence Intensity During Storm Conditions Over the North Sea," *J. Geophys. Res.* 92, 13137-13149.

Geernaert, G.L., P.S. Guest, and K.L. Davidson (1989), "Ducting Characteristics Over the Marginal Ice Zone of the East Greenland Sea," unpublished report, Naval Research Laboratory.

Geernaert, G.L., W.J. Plant and D. Schuler (1988), "Radar Cross-Section Dependence on Environmental Parameters During FASINEX," Proceedings of the AMS Conference on Air-sea Interaction.

Geernaert, G.L. (1989), "Bulk Measurements of Air-Sea Fluxes, in *Surface Waves and Fluxes: Current Theory and Remote Sensing*, Geernaert and Plant, eds., (Kluwer Press, Dordrecht, Holland) in press.

Geernaert, G.L. (1989), "On Diabatic Wind Stress Estimates with Wave Feedback Effects for Remote Sensing in the Coastal Zone," in preparation.

Goroch, A. (1982), "Aircraft Measurements of PBL Depth and Sea Surface Temperature Across the Gulf Stream Wall," internal NEPRF report.

Johannessen, J.A. (1989), Nansen Center for Remote Sensing, Bergen, personal communication.

Katsaros, K.B., S. Smith, and W. Oost (1987), "The HEXOS Experiment," Internal Report, University of Washington, Seattle.

Kerr, D.E., ed. (1951), *Propagation of Short Radio Waves*, Chs. 2, 3, and 4 (McGraw Hill Publishers, NY).

Li, F., D.E. Weissmann, W. Large, and K.L. Davidson (1989), "Dependence of Radar Cross-Section on Wind Stress and Wave Slope During FASINEX," in press *J. Phys. Oceanogr.*

Martin, F.L., and F.E. Wright (1963), "Radar-Ray Refraction Associated with Horizontal Variations in the Refractivity," *J. Geoph. Res.* 68, 1861-1869.

Panofsky, H.A., and J.A. Dutton (1984), *Atmospheric Turbulence* (Academic Press, New York).

Richter, J. (1979), "Integrated Refractive Effects Prediction System (IREPS) and Environmental/Weapons Effects Prediction System (E/WEPS)," Proceedings of the Conference on Atmospheric Refractive Effects Assessment, San Diego, CA.

Schleher, J.S. (1982), "Tilted Refractive Surfaces at Eglin Air Force Base, Florida," *Radio Sci.* 17, 1281-1284.

Smith, S.D. 1980, "Wind Stress and Heat Flux Over the Ocean in Gale Force Winds," *J. Phys. Oceanogr.* 10, 709-726.

Smolinski, S.P. (1988), "Marine Boundary Layer Depth and Relative Humidity Estimates Using Multispectral Satellite Estimates," Masters thesis, Naval Postgraduate School, Monterey, CA, 93943-5000.

Thompson, W.T. (1987), "The Surface Evaporation Duct Height Product: An Evaluation," NEPRF Technical Report TR 87-05.